EASR

Engineering and Applied Science Research

https://www.tci-thaijo.org/index.php/easr/index

Published by the Faculty of Engineering, Khon Kaen University, Thailand

Europium-doped soda lime borosilicate glass from agricultural wastes: Physical, structural, and optical properties

Serifat O. Adeleye*[1)], Adekunle A. Adeleke[2)], Petrus Nzerem[3)], Adebayo I. Olosho[4)], Esther N. Anosike-Francis[2)], Waliyi A. Adeleke[2)], Abdulkarim M. Hamza[5)] and Prabhu Paramasivam[6, 7)]

[1)]Department of Industrial Chemistry, Nile University of Nigeria, Abuja FCT, Nigeria
[2)]Department of Mechanical Engineering, Nile University of Nigeria, Abuja FCT, Nigeria
[3)]Department of Petroleum and Gas Engineering, Nile University of Nigeria, Abuja FCT, Nigeria
[4)]Department of Chemistry, African University of Science and Technology, Abuja FCT, Nigeria
[5)]Department of Physics, Federal University of Lafia, Nasarawa State, Nigeria
[6)]Department of Mechanical Engineering, Mattu University, Mettu, Ethiopia
[7)]Centre of Research Impact and Outcome, Chitkara University, Rajpura 140417, Punjab, India

Received 13 August 2024
Revised 11 February 2025
Accepted 13 February 2025

Abstract

Wheat husks and eggshells, while often regarded as waste, are available in millions of tons. Despite their status as by-products, these materials possess significant potential for various applications. Thus, this study explores the possibility of agricultural waste as a source of bio-silicate materials for glass production. Bio-silicate was extracted from leached wheat husks, and lime was obtained from eggshells. Europium-doped soda-lime borosilicate glasses were fabricated using the melt-quenching method having a chemical composition of $30Na_2O$-$(40-x)B_2O_3$-$20SiO_2$-$10CaO$-xEu_2O_3 wherein x varied from 0.01 to 0.05 mol%. Chemical oxide compositions of wheat husk ash (88.64% SiO_2) and calcined eggshell (91.30% CaO) were determined using X-ray fluorescence (XRF). Functional groups were confirmed by Fourier transform infrared (FTIR) spectroscopy. It was confirmed by X-ray diffraction (XRD) that the glasses were amorphous. The glasses exhibited 2.61 to 3.03 g/cm³ densities and molar volumes of 10.91 to 14.37 cm³, increasing with higher europium doping levels, indicating a denser glass network. Optical features were characterised using Ultraviolet-visible (UV-Vis) spectroscopy, revealing direct band gaps ranging from 3.55 to 4.90 eV and indirect band gaps from 0.40 to 1.99 eV. Glasses doped with 0.05 mol fraction Eu^{3+} showed the highest density, molar volume, and Urbach energy, suggesting suitability for UV-absorbing materials and high-energy photonic devices. Due to their unique emission properties under various excitation wavelengths and adaptable optical band gaps, the europium-doped borosilicate glasses derived from agricultural waste are useful in optical devices such as white LEDs.

Keywords: Bio-silicate materials, Europium-doped, Borosilicate glass, Agricultural wastes, Melt-quenching technique

1. Introduction

Borosilicate glasses have garnered significant attention in industrial and medical fields over the past few decades due to their high ionic conduction, mechanical and thermal stability, and optical transparency [1]. These properties make borosilicate glasses suitable for various advanced applications, including optoelectronics and photonics. The optical quality of borate glasses can be improved by modifying borate structural units from BO_3 to BO_4, a process facilitated by incorporating alkali ions such as CaO and Na_2CO_3. These ions improve chemical stability and physical properties of the glass network, making it more suitable for technological applications [2, 3]. Traditional borate glasses, characterised by high phonon energy, low viscosity, and moisture resistance, are generally unsuitable for optoelectronic devices. However, incorporating alkali oxides into the borate network mitigates these drawbacks, thereby, enhancing the performance of the material [4, 5]. Moreover, borosilicate glass serves as an excellent medium for incorporating various transition metals and lanthanide ions, further expanding its application potential. The silica and the alkali such as calcium oxide can be obtained from agricultural waste, offering an environmentally friendly solution to waste disposal issues while providing valuable raw materials for glass production. Wheat husks are a novel source of SiO_2 due to their high silicon content, while eggshells, containing 98% calcium carbonate, offer a convenient and cost-effective source of CaO [6]. Activators and/or modifiers that are alkaline or alkaline earth have been added to make borate glasses more effective.

Research indicates that glasses enhanced with rare earth ions (REIs) show a possibility for developing luminescent devices, fibre, and waveguide amplifiers for optical transmission networks, infrared to visible up-converters, colour display devices, optoelectronic devices like visible short-wavelength lasers, and high-density frequency domain optical data storage [7-10]. REIs exhibit fascinating

*Corresponding author.
Email address: serifatolamide@gmail.com
doi: 10.14456/easr.2025.15

luminescent properties due to their narrow emission lines from f-f transitions, making them useful for various applications. The REI europium (Eu^{3+}-$4f^6$) is particularly notable for its almost monochromatic electric dipole emission transition and high luminescence efficiency [11], making it an excellent candidate for red-emitting photoluminescence [1]. The local environment in different glasses can be assessed using the Eu^{3+} ion, which significantly alters the optical and magnetic characteristics of oxide glass hosts. Research has shown that REIs form a glass matrix that facilitates energy transfer between nearby ions. The energy level structure of Eu^{3+} is highly sensitive and reactive to fluorescence within the glass matrix, making it ideal for studying the local structure of rare earth ions in glasses [12]. Numerous studies have explored the environments of REIs in silicate glasses [13-17]. For instance, Gowda et al. [18] examined the lead borotellurite glasses doped with europium trioxide and their structural, thermal, and spectroscopic characteristics, concluding that these glasses possessed good thermal and glass stability. Mariselvan et al. [19] reported on the luminescence and optical properties of barium lithium fluoroborate glasses doped with europium, highlighting their potential for red-coloured lasers and display devices. Umar et al.[20] analysed the optical, structural, and physical characteristics of rice husk silicate borotellurite (Er-doped RHSBT) glasses doped with erbium, noting a decrease in reflectivity and polaron radius with increased REI concentration, indicating reduced optical energy loss to reflection. This study focuses on the extraction of silica from wheat husk and calcium oxide from eggshells for integration into a glass matrix. Additionally, it investigates the effects of europium doping on the structural and optical properties of borosilicate glass. The incorporation of these waste-derived materials aims to improve the glass properties and offer an environmentally sustainable solution to waste disposal. The optical, structural and physical properties of the resulting soda-lime borosilicate glasses were comprehensively studied.

2. Materials and methods

2.1 Materials

The wheat husk utilized in this investigation was obtained from a Maiduguri farm in Nigeria, and the chicken eggshell waste was collected from restaurants in Suleja, Nigeria. Diboron trioxide was obtained from Sigma-Aldrich (Germany), and Europium (III) oxide and sodium carbonate were obtained from Merck (USA). All chemicals were utilized just as supplied without any additional purification.

2.2 Methods

2.2.1 Extraction of bio-Silicates from wheat husk

The husk underwent a series of steps to extract silica from the wheat husk. The wheat husk was initially thoroughly cleaned with regular water and then distilled water. The sample was drained and then leached in 1M hydrochloric acid for approximately 2 h. It was then stirred and heated to 110℃ for 3 h. Following the removal of acid, distilled water was used to rinse the husk after which it was oven-dried at 105 °C for approximately 3 h. After that, dried wheat husk was subsequently ashed in a muffle furnace at 800 °C for 5 h to obtain the wheat husk ash (WHA) [21, 22].

2.2.2 Extraction of calcium oxide (CaO) from eggshell

CaO was obtained from discarded chicken eggshells (CES). The shells were initially cleaned to get rid of any dirt or other debris that might have adhered to the outside of the shell. After the internal white membrane was removed, the shell was thoroughly cleaned with distilled water and then dried at 105°C for 3 h in the oven to remove moisture from the eggshell. The dried eggshells were crushed until smooth. The eggshell was heated to 900°C for 5 h in a furnace [23, 24].

2.2.3 Glass fabrication

Figure 1 represents the flowchart of the entire glass production methods. The chemical formula $(40\text{-}x)B_2O_3\text{-}30Na_2O\text{-}20SiO_2\text{-}10CaO\text{-}xEu_2O_3$ was utilized to prepare a range of borosilicate glasses doped with europium where x= 0.01, 0.02, 0.03, 0.04 and 0.05 mol% using conventional melt quenching techniques [25-27]. 13 g of powdered chemicals were weighed using molar ratio of $30Na_2O\text{-}(40\text{-}x)B_2O_3\text{-}20SiO_2\text{-}10CaO\text{-}xEu_2O_3$. The weighed chemicals were combined and then stirred for 30 minutes to ensure the mixture was homogenous. After preheating the homogeneous mix for 1 h at 400 °C to remove any residual water, it was heated to 950 °C for an additional 2 h to allow the sample to melt. The glass was annealed for five hours at 250°C to eliminate thermal and mechanical stress before glass casting. Silicon carbide was used to polish the prepared glass (Figure 2). Table 1 depicts the chemical composition of the fabricated glass samples.

Table 1 Chemical composition (%) of Europium doped sodalime borosilicate glass

Sample code	B_2O_3	Na_2O	SiO_2	CaO	Eu_2O_3
NaCaBSi	40	30	20	10	0.00
NaCaBSiEu1	39	30	20	10	1.00
NaCaBSiEu2	38	30	20	10	2.00
NaCaBSiEu3	37	30	20	10	3.00
NaCaBSiEu4	36	30	20	10	4.00
NaCaBSiEu5	35	30	20	10	5.00

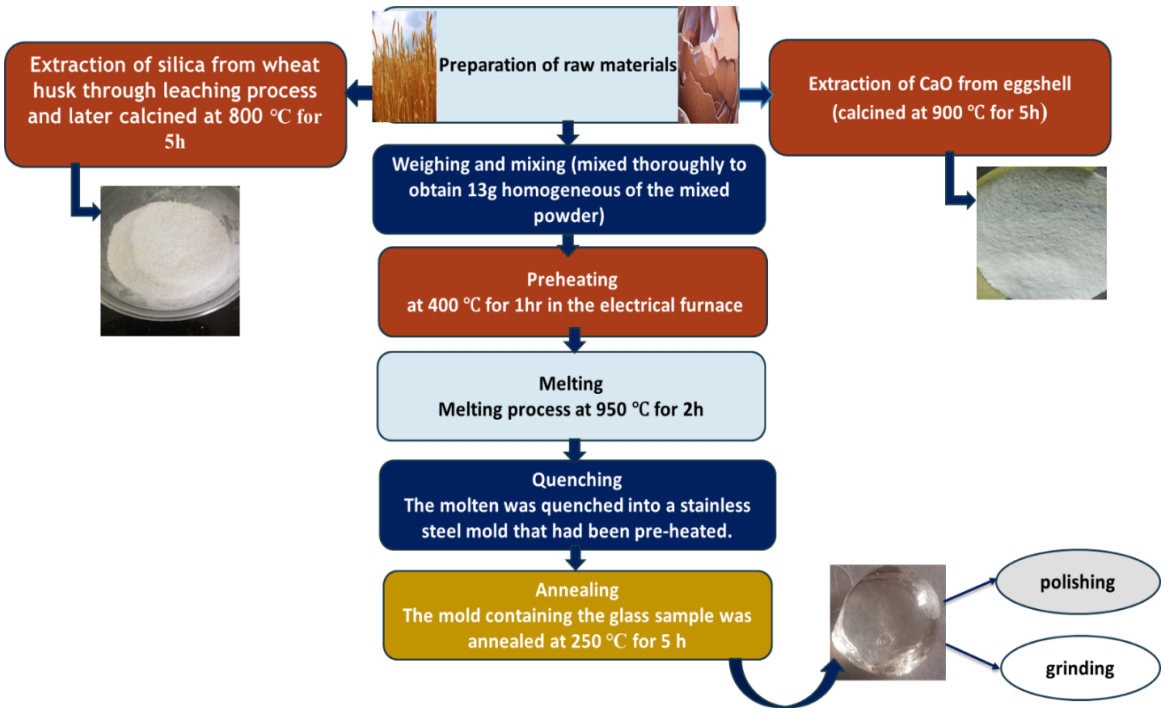

Figure 1 Flow diagram for the procedure

Figure 2 A typical image of soda-lime borosilicate glass

2.3 Characterization of raw materials and produced glasses

2.3.1 X-Ray fluorescence analysis

The elemental compositions of WHA and CES were determined using an X-ray fluorescence meter (PanAlytical Epsilon 4). The sample was ground into a powder using an agate pulverizing device (planetary micro mill pulverisette 7). The resulting spectrum described the elemental composition of the material.

2.3.2 Physical analysis

Glass sample densities were determined using the Archimedes principle and an automated electronic densimeter measurement device with serial numbers SO.20230409001, 300A. Equation (1) was used to obtain the density;

$$\rho_{sample} = \frac{W_{air}}{W_{water}} \rho_{water} \quad (1)$$

The molar volume of every sample was determined using Equation (2).

$$V_m = \frac{M_w}{\rho_{sample}} \quad (2)$$

where ρ_{sample} = sample density, ρ_{water} = density of water, w_{Air} = weight of sample in air, w_{water} = weight of sample in water, and M_w = molecular weight of the glass sample respectively

2.3.3 X-Ray diffraction analysis

The Rigaku Miniflex X-ray diffractometer was used to identify the phase of CES, WHA, and glass samples. The X-ray diffractometer has a fixed acceleration voltage of 30 kV, a fixed current of 15 mA, a scan range of 2θ = 2° - 145°, and a scan speed of 0.01-100 °/min. The source of X-rays is a copper anode (**λ** Cu Kα, radiation = 1.5406Å). The diffraction patterns were analyzed using the Joint Committee on Powder Diffraction Standards (JCPDS).

2.3.4 Fourier transform-infrared (FTIR) analysis

An Agilent Technologies CARY, INFrared 630 Fourier Transform-Infrared Spectrometer (FTIR) at Ahmadu Bello University (ABU), Zaria, Nigeria. Was used to identify the functional to identify the functional groups. Each sample was crushed into a fine powder before preparations. The sample FTIR spectra were obtained in the 4000 – 400 cm-1 range and at a resolution of 4 cm^{-1} using the KBr pellet method.

2.3.5 UV-Vis analysis

The refractive index of the glass samples was estimated from the absorption spectra based on the fundamental relations as outlined in this section. The optical absorption was measured using a Cary series UV–Vis NIR spectrophotometer (Shidmazu, model UV-3600) with a spectral resolution of 0.2 nm. The optical energy bandgap (Eg) for direct and indirect transitions and the Urbach energy (ΔE) for the synthesized samples were evaluated using the fundamental relations provided by Aliyu et al. [28].

The absorption coefficient α (v) as a function of photon energy and the Davis and Mott formula were used to compute the optical band gaps (direct and indirect) [20].

The expression for α(v) is given in Equation (3):

$$\alpha(v) = B\frac{(hv - E_{opt})^n}{hv} \tag{3}$$

where E_{opt} is the optical band gap, n is a number, with n = 2 for indirect and n = 1/2 for direct allowed transitions, and B is a constant. The value of α (υ) is the absorption coefficient obtained using Equation (4);

$$\alpha(v) = 2.303\frac{A}{t} \tag{4}$$

where t is the sample's thickness and A is the value of the corresponding optical absorbance. The optical band gap values were obtained by extrapolating the linear part of the curves at $(\alpha hv)^2 = 0$ and $(\alpha hv)^{1/2} = 0$ for direct and indirect transitions, respectively.

The localized states' width corresponding to an optical transition between the extended state in the conduction band above the mobility edge and the localized tail states in the neighbouring valence band is known as the Urbach energy (ΔE). It is given by Equation (5).

$$\alpha(v) = B\exp^{hv/\Delta E} \tag{5}$$

where β is a constant and ΔE is the band tailing parameter. The inverse of the slope of ln α versus the *h*v plot (Equation 6) was used to calculate the ΔE.

$$\ln\alpha = \frac{hv}{\Delta E} \tag{6}$$

The refractive index of the glass sample was determined utilizing Tauc's method in Equation (7) i.e relationship between refractive index (n), and optical band gap

$$\frac{n^2-1}{n^2+2} = 1 - \sqrt{\frac{E_{opt}}{20}} \tag{7}$$

where E_{opt} is the value of the indirect band gap and n is the refractive index.

The optical parameters were determined using the refractive index, and the n value was obtained [29, 30]. The average molar refraction of isotropic substances is given by Equation (8).

$$R_m = \frac{(n_0^2-1)}{(n_0^2+2)}V_m \tag{8}$$

Equation (9) was used to determine the oxide ions' electronic polarizability according to their refractive index. The electronic polarizability is proportional to the molar refraction [31]. This was demonstrated by applying Avogadro's number to Equation (10):

$$\alpha_m = \left(\frac{3}{4\pi N_A}\right)R_m \tag{9}$$

where α_m is the electronic polarizability, N_A represents Avogadro's number and R_m represent molar refraction. With α_m ($Å^3$), This Equation may be modified to:

$$\alpha_m = {R_m}/{2.52} \quad (10)$$

Polarion radius (r_p): The polaron radius (rp) for the glass samples was calculated using Equation (11) as described by Hegde et al. [10].

$$r_p(\text{Å}) = \frac{1}{2}\left(\frac{\pi}{6N}\right)^{1/3} \quad (11)$$

The interionic distance was calculated using Equation (12)

$$r_i(\text{Å}) = \left(\frac{1}{N}\right)^{1/3} \quad (12)$$

where N is the concentration of the Eu^{3+} ion

Equation (13) was used to determine the field strength (F_s) surrounding the Eu^{3+} ion:

$$\text{Field strength } (F_s)\ (\text{cm}^{-2}) = \left(\frac{Z}{r_p^2}\right) \quad (13)$$

The subsequent relation in Equation (14) was used to obtain the dielectric constant (ε)

$$\varepsilon = n^2 \quad (14)$$

where n is the refractive index.

Reflection loss (R_L) and transmission coefficient (T): Equations (15) and (16) display the reflection loss and transmission coefficient, which were calculated using Fresnel's formula and the refractive index of the produced glasses, respectively [28].

$$T = \frac{2n}{n^2+1} \quad (15)$$

Fresnel's formula was utilized to calculate the reflection loss from the glass surface based on the refractive index.

$$R_L = \left[\frac{(n-1)}{(n+1)}\right]^2 \quad (16)$$

Optical electronegativity (χ): Optical electronegativity is calculated theoretically based on energy band gap using Equation (17) [32].

$$\Delta\chi = 0.2688 \times E_{opt} \quad (17)$$

where E_{opt} represents the simple oxide's energy gap.

Metallization criterion (M). Equation (18) was utilized to evaluate the glass insulating performance by using the metallization criteria. The metallization theory of Herzfeld states that materials tend to be metallic or insulating if Rm/Vm >1 and Rm/Vm <1. Thus, the metallization (M) was obtained from Equation (18) [33].

$$M = 1 - \frac{R_m}{V_m} \quad (18)$$

Equations (19) and (20) were used to the refractive index, M(n), and energy band gap, M(Eg), which are used to determine the metallization criteria [34].

$$M(n) = 1 - \left[\frac{(n_o^2-1)}{(n_o^2+2)}\right] \quad (19)$$

$$M(E_g) = \sqrt{{E_g}/{20}} \quad (20)$$

Optical electronegativity-based oxide ion polarizability ($\alpha_{O^{2-}}$) and optical basicity (Λ): Glasses oxide ion polarizability can be estimated based on the optical electronegativity computed from the refractive index [35]. Equation (21) illustrates the optical electronegativity estimated from the refractive index by Zhao et al. [36] to predict the oxide ion polarizability of oxide glasses.

$$\alpha_{O^{2-}} = 3.5 - 0.9\chi_{glass} \quad (21)$$

According to Reddy et al. [37] and Moustafa and Elkhateb [38], there is an excellent correlation exists between the oxide ion polarizability and average electronegativity.

The optical basicity of the samples is estimated from Equation (22) [39]

$$\Lambda = 1.7 - 0.5\chi \quad (22)$$

3. Results and discussion

3.1 Characterization of raw materials

Table 2 displays the oxide content of wheat husk ash (WHA) and calcined eggshells (CES) as determined by X-ray fluorescence spectroscopy. WHA contains 88.64% SiO_2, while CES is composed of 91.3% CaO. The silica content of WHA aligns with the recommended range of raw materials suitable for glass fabrication, as stated by Hamza et al. [22] and Umar et al. [20]. This high silica content makes WHA a potential precursor for the glass industry.

The IR spectra of CES, shown in Figure 3a, exhibit characteristic bands at approximately 3600 cm^{-1}, attributed to OH in $Ca(OH)_2$, formed due to reactive moisture adsorption [40-42]. The band located at 864 cm-1 is linked to Ca–O [43, 44]. The spectra of WHA (Figure 3b) display characteristic asymmetric peaks at 1058 cm^{-1} due to the stretching of O-Si-O and the Si-OH stretching vibration of the silanol group around 782 cm^{-1} [45]. These findings are consistent with the outcomes of Awogbemi et al. [41] and Gouran et al. [46]. The FTIR results confirm that both eggshells and wheat husk ash are potential glass formers.

Table 2 Chemical composition of WHA and calcined eggshell (CES).

Elemental composition	WHA (%)	CES (%)
SiO_2	88.60	0.35
CaO	1.15	91.30
Fe_2O_3	0.85	-
Al_2O_3	2.20	0.10
P_2O_5	3.82	0.60
K_2O	0.18	-
TiO_2	0.15	-
MgO	-	0.26
CuO	-	0.00

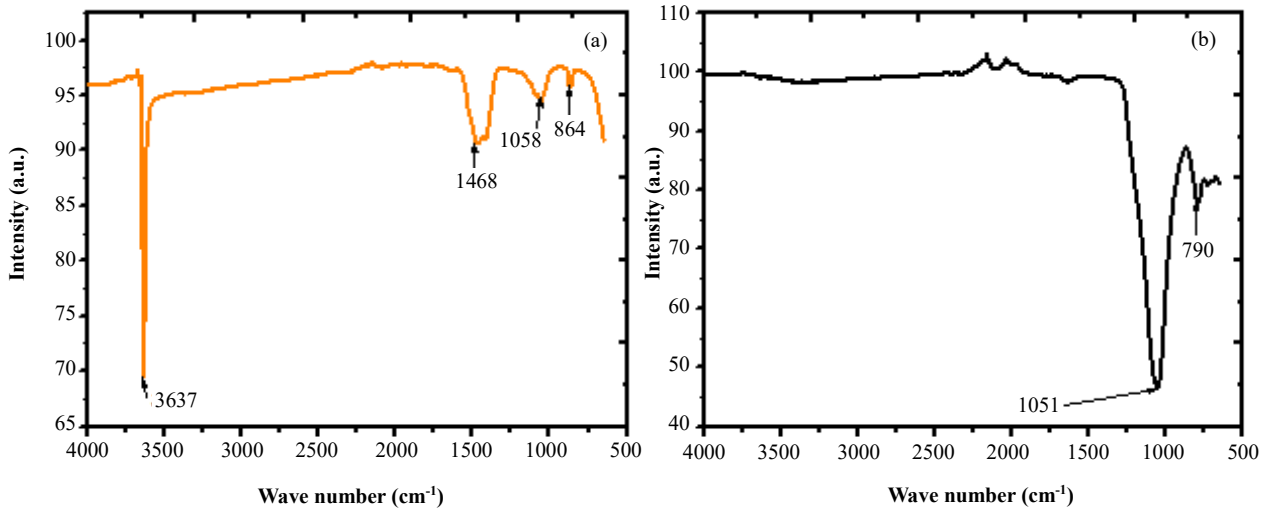

Figure 3 FTIR spectra of (a) CES and (b) WHA

3.2 Physical properties of the produced glasses

A deep understanding of dopant-induced modifications in material behaviour is critical, particularly for europium-doped soda-lime borosilicate glass. A comprehensive physical analysis is essential to unravel these effects, providing valuable insights into the structural, optical, and mechanical properties of the material. This knowledge is fundamental for optimizing performance, enhancing durability, and ensuring reliability in specialized applications.

3.2.1 Molar volume and density

The impact of Eu^{3+} concentration on the molar volume and density of the glass is depicted in Figure 4. The molar volume and density of the glass increased as the Eu^{3+} concentration increased. This signifies that the glass network becomes more rigid as Eu^{3+} content increases [47]. The addition of europium atoms which are heavier relative to other constituents contributes to this phenomenon [20, 26, 48-51]. The incorporation of Eu^{3+} ions resulted in a higher proportion of tetrahedral BO_4 units and bridging oxygens (BOs) which enhances the glass network's structural integrity [26, 47, 48, 52]. The network strengthening contributes to the observed increased density of the glass produced. The glass molar volume also increases with higher Eu^{3+} concentrations because of the replacement of the atoms of boron by larger Eu^{3+}, leading to expanded glass structures [26, 46]. This phenomenon suggests an occurrence of non-bridging oxygens (NBOs) and further elucidates the impact of europium doping on the glass matrix.

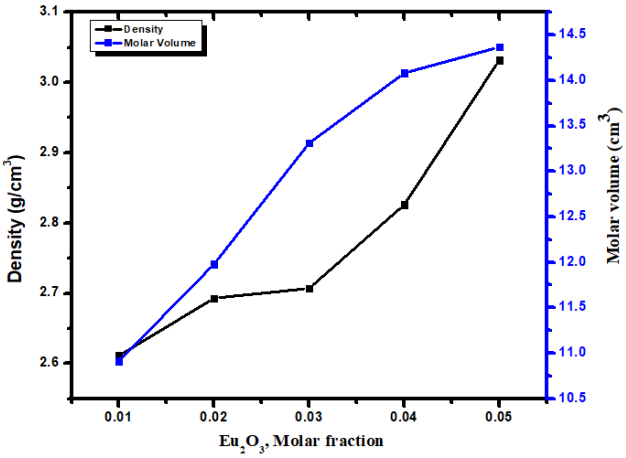

Figure 4 Molar volume and density of the produced glasses

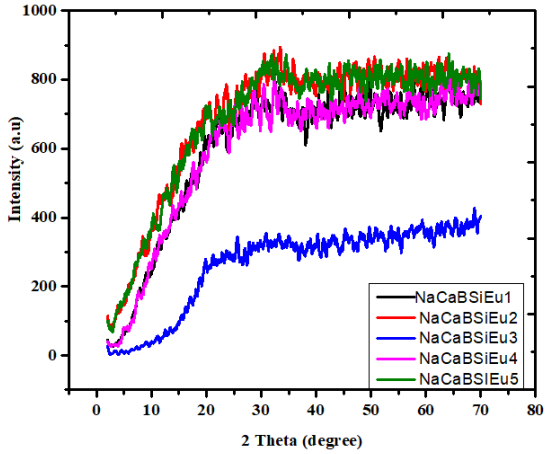

Figure 5 XRD spectra patterns for europium oxide doped soda-lime borosilicate glasses.

3.3 Structural properties of the produced glasses

3.3.1 X-ray diffraction analysis

The XRD patterns of the produced glasses shown in Figure 5 exhibit a broad hump within the 20°–30° range, with no detectable crystalline peaks, confirming their amorphous nature [53]. The absence of crystallization peaks or long-range periodic order in the glass structure as noted in previous studies [11, 22] further supports this conclusion. Therefore, it can be definitively stated that the glass maintains an amorphous structure due to the lack of long-range periodic order

3.3.2 FTIR Analysis

The glass sample FTIR spectrum, presented in Figure 6, reveals the functional groups present and indicates a structural rearrangement due to the addition of Eu^{3+} to the host matrix. The band shows the Si-O-Si symmetric stretching of the bridging oxygen between the tetrahedral phases at around 750 cm^{-1} [54, 55]. The stretching vibrations of BO_4 units in di-borate groups are attributed to the band between 900 and 950 cm^{-1}. The band at about 1369 cm^{-1} is associated with symmetric B–O stretching vibrations in BO_3 units belonging to the orthoborate, pyroborate, and metaborate groups [10, 31]. The bands at 1190-1199 cm^{-1} are linked to B-O vibrations in BO_3 units within boroxol rings [28]. This affirms boroxol rings (B_3O_6) splitting into BO_3 and BO_4 units. Therefore, by forming bridging oxygens (BOs) in the glasses that were produced, the action of Eu^{3+}, which acted as a "network strengthener" in the produced glasses by bridging oxygens, is responsible for the structural changes and compactness of the glass.

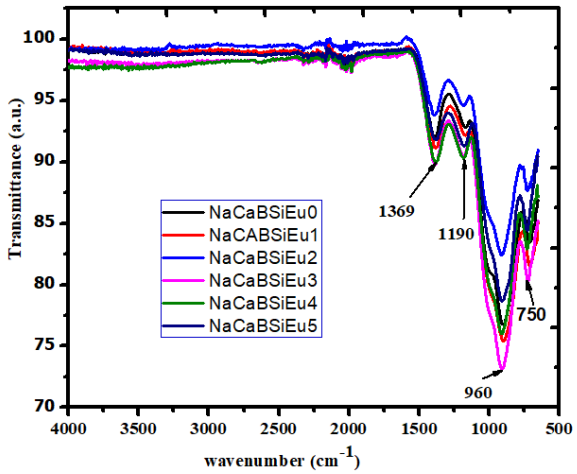

Figure 6 The FTIR spectra of the Eu^{3+} doped NaCaBSi glass samples.

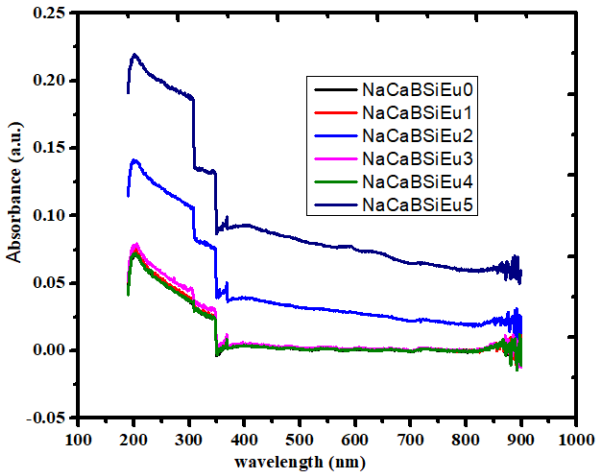

Figure 7 Absorption spectrum of 0.00-0.05Eu mol% of the produced glass

3.4 Optical properties of the produced glasses

3.4.1 Optical band gap and Urbach energy

Glass structures are ideal hosts for rare earth ions like Europium (Eu^{3+}) due to their heterogeneously widened optical conversion line widths and simple compositional changes. Europium, with the electronic configuration [Xe] $4f^n$ $6s^2$, has partially filled 4f shells. Absorption peaks from infrared to ultraviolet areas become visible as a result of these intra-4f transitions. Visible and near-IR absorption corresponds to transitions between f-f energy levels, while UV absorption results from transitions from the 4f to the higher

energy 5d level [56]. Figure 7 shows the UV-near infrared absorption spectra of Eu^{3+} doped borosilicate glasses with varying concentrations of the dopant (0.00 to 0.05 mol%) across the 200-1000 nm wavelength range. The glasses absorb light in the visible and near-infrared regions due to transitions from the $^7F_0$ and $^7F_1$ to higher energy levels. The absorption peak around 200 nm is likely due to the charge transfer band associated with Eu^{3+} ions, signifying transitions related to the interaction between the europium ions and the glass matrix. Absorbed photons at approximately 368 nm and 404 nm correspond to the $^7F_0 \rightarrow {}^5D_4$ and $^7F_0 \rightarrow {}^5L_6$ transitions, respectively [57, 58], indicating specific electronic transitions within the europium ion's 4f orbital configuration. These absorption characteristics are consistent with other studies involving different glass matrices doped with rare earth ions, confirming the behaviour of europium-doped glasses [59-61].

The lack of a sharply defined optical absorption edge in the spectra indicates the glassy nature of the samples. In amorphous materials, the cations affect the indirect band, significantly influencing properties such as refractive index and polarizability, while the glass-forming anions influence the conduction band [28]. The intensity of the absorption bands increased with higher Eu^{3+} concentrations, due to a greater number of absorbing centres within the glass matrix, leading to a higher absorption coefficient. This enhanced Eu^{3+} concentration boosts charge transfer transitions, particularly from oxygen ligands to Eu^{3+} ions, resulting in stronger absorption bands [62]. At higher concentrations, interactions between Eu^{3+} ions further increase absorption intensity due to cooperative effects, although excessive concentrations may eventually cause quenching [63]. Additionally, increasing Eu^{3+} concentration can modify the local glass structure, potentially reducing non-bridging oxygen atoms and altering the glass network, which also affects absorption properties. Tauc's plot, derived from the absorption coefficient data, was used to determine the optical band gaps of the glass samples, as shown in Figure 8. The direct band gap, plotted as $(\alpha h\nu)^2$ against hv, ranges from 3.55 to 4.90 eV, indicating high-energy transitions that require higher photon energies. These values suggest that the glass samples have tightly bound electronic states, making them suitable for UV-absorbing materials or high-energy photonic devices [64]. In contrast, the indirect optical band gap, plotted as $(\alpha h\nu)^{1/2}$ against hv, ranges from 0.40 to 1.99 eV. This lower energy range indicates that less energy is needed for indirect transitions, covering the infrared to visible regions. This suggests potential applications in photonic devices operating at lower energies, such as solar cells or infrared detectors [65, 66].

These findings demonstrate that the glass samples possess diverse optical properties, making them versatile for various technological applications based on their specific band gap energies. Europium-doped borosilicate glasses, in particular, show promise for use in white light-emitting diodes (LEDs) due to their ability to produce orange-red emissions when excited by multiple wavelengths, making them suitable candidates for white LED applications [11, 67].

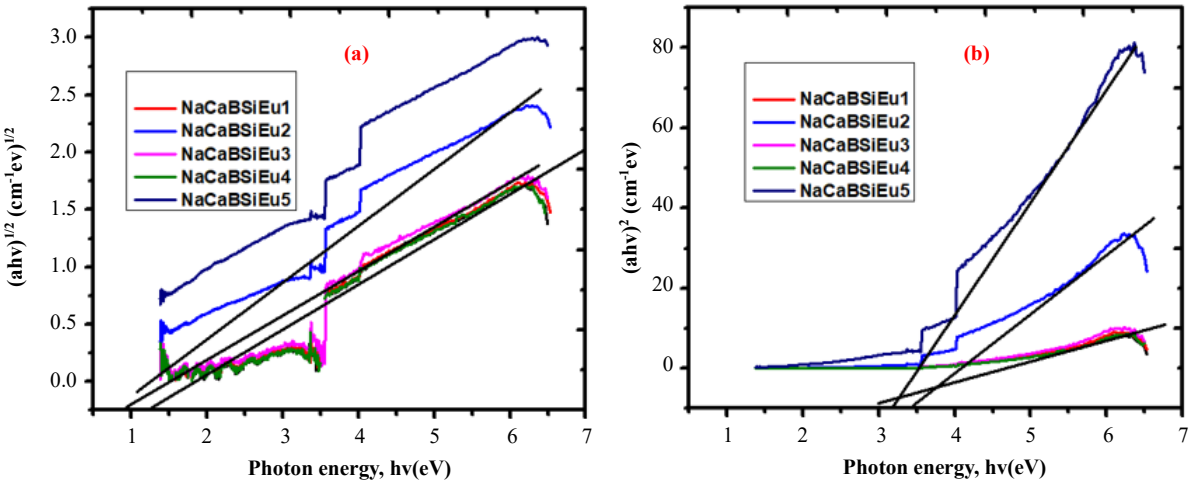

Figure 8 Plot of (a) $(\alpha h\nu)^{1/2}$ against hv and (b) $(\alpha h\nu)^2$ against hv for europium doped soda-lime borosilicate silicate glasses

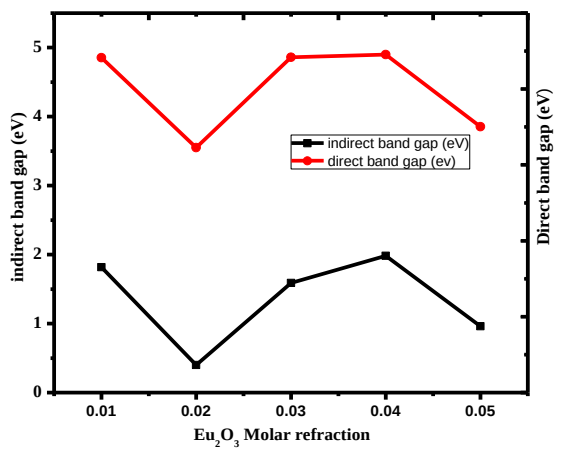

Figure 9 Indirect and direct optical band gap of europium-doped soda-lime borosilicate glasses

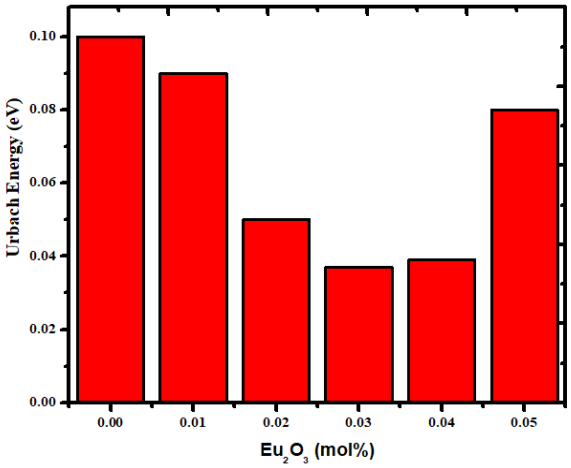

Figure 10 Urbach energy as a function of europium-doped borosilicate glasses

Figure 9 illustrates that the indirect and direct optical band gaps of the glass samples follow opposite trends with increasing Eu^{3+} concentration. While the indirect band gap increases, the direct band gap decreases. This behaviour can be attributed to structural modifications within the glass matrix induced by europium doping, which influences the electronic band structure and the nature of optical transitions. These variations in the optical band gaps are attributed to structural changes induced by the addition of Eu^{3+}, which produces non-bridging oxygen (NBO) sites, modifying the glass structure, consistent with FTIR data. This aligns with previous studies that reported similar results, indicating a less ordered glass structure [19, 29, 50, 68-70]. Azlan et al. [68] explained that the decrease in optical band gap energy is due to the weaker bond strength of europium oxide (Eu–O) compared to boron oxide (B–O). Azlan et al. [68] and Saddeek et al. [49] As the dopant concentration increases, the direct band gap narrows from 4.90 to 3.85 eV, and the indirect band gap narrows from 1.98 to 0.96 eV. Within the glass system, this narrowing is linked to an increase in free electrons [71], resulting from the increasing number of NBO atoms [72]. Therefore, the internal structure and chemical composition of the glass samples significantly impacts the optical band gaps.

Figure 10 shows the Urbach energy of the glass samples, a key parameter for assessing the level of disorder in the glass structure. As the Eu^{3+} content increases, the Urbach energy also increases, indicating a higher level of atomic disarrangement within the glass. This rise in Urbach energy (ΔE) is associated with an increase in disorder and defect states in the glass structure, leading to a higher number of non-bridging oxygen and BO_3 units [29, 71].

3.4.2 Refractive index (n), Molar refraction (R_m), and electronic polarizability (α_m).

The produced glass samples were assessed for their optical viability, focusing on the refractive index and electronic polarizability. As illustrated in Figure 11a, the refractive index of the glass initially decreases from 0.00 to 0.03 Eu mol% before increasing from 0.04 to 0.05 Eu mol%. The observed decrease in refractive index can be attributed to the incorporation of a modifier, which reduces the number of nonbridging oxygens (NBOs) within the glass network. This reduction in high-polarizability NBOs results in a lower refractive index as the europium oxide concentration increases. Conversely, the subsequent increase in refractive index is associated with the addition of Eu^{3+} ions, leading to structural modifications, specifically the transition from BO_4 tetrahedral units to BO_3 triangular units. Similar observations were reported by Azlan et al. [68] and Zagrai et al. [71]. The creation of NBO, which is more polarizable than BO, also contributes to the higher refractive index, consistent with findings from studies involving erbium-doped glasses [68]. Figure 11b illustrates that the glasses' molar refraction and electronic polarizability increase as the Eu^{3+} concentration rises from 0.01 to 0.05 mol%, with mol% increasing from 9.56 to 11.22 and polarizability from 3.79 to 4.45. This suggests that the glasses become highly polarized owing to the greater amount of non-bridging oxygen, which has higher polarizability than bridging oxygen, as Eu^{3+} content increases. The findings indicate that the polarizability of the glass materials, in addition to density, affects the refractive index. NBO tends to polarize more than BOs, which explains the observed increase in refractive index and polarizability [19, 29, 31, 70].

The structural alterations seen in soda-lime borosilicate glass can be explained by the Eu^{3+} function as a network modifier in the glass. Eu^{3+} ions break bonds and integrate into the glass network by forming symmetric NBO ions. This results in a restructuring of the internal glass network, a decrease in bandgap energy, an increase in refractive index, and an increase in the degree of disorder and defect states within the glass network.

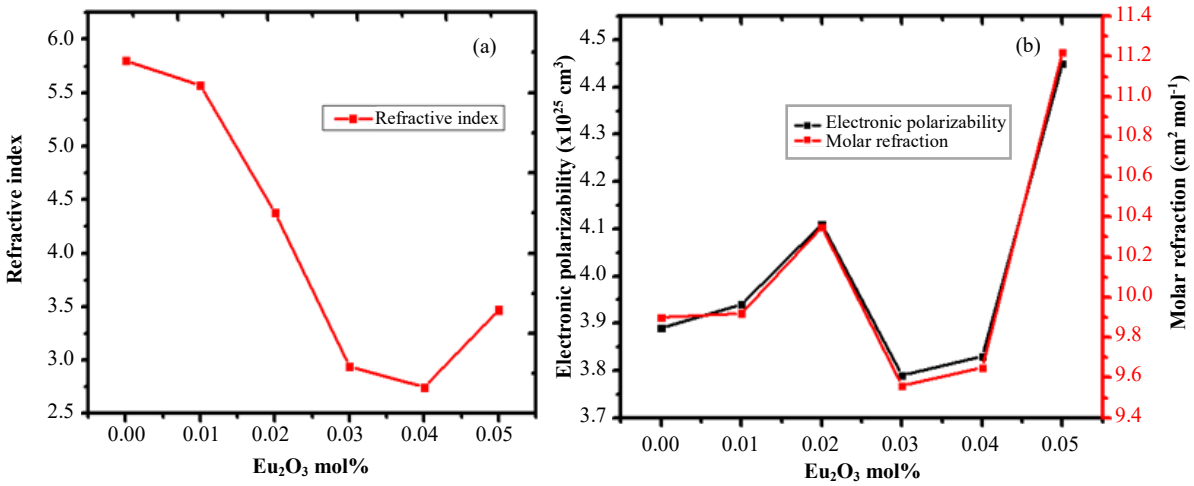

Figure 11 (a) The refractive index and (b) electronic polarizability/molar% of the produced glass

3.4.3 Polarion radius (r_p), Internuclear distance (r_i), and Field strength (F_s)

The polaron radius is used to study the polar interaction between an electron and longitudinal optical phonons. This radius represents the linear displacement field of atoms or ions surrounding a polaron. A polaron is regarded as large when its radius exceeds the material's lattice constant and small when its radius closely matches the lattice constant [20]. Figures 12(a) and 12(b) show the polaron radius (r_p), internuclear distance (r_i), and field strength (F_s) of a glass series doped with Eu^{3+}. The decrease of the internuclear distance and the polaron radius continuously with increasing Eu_2O_3 content. In contrast, the field strength increases with higher Eu_2O_3 concentration. This pattern indicates an enhancement in the glass network's polarizability and compactness, potentially leading to improved electrical conductivity. The robust bond formation between Eu and O contributes to the intensified field strength around Eu^{3+}, resulting in the observed reduction in the polaron radius [20]. The increase in Eu^{3+} ion concentration likely corresponds to the diminishing (r_p) with escalating Eu_2O_3 content. This trend is due to the bolstered field strength surrounding Eu^{3+} ions, resulting from heightened bond strength and a reduced average distance between europium and oxygen atoms. The polaron classification remains small, as indicated by the calculated values being below the lattice constants of the various oxides within the glass [10, 73].

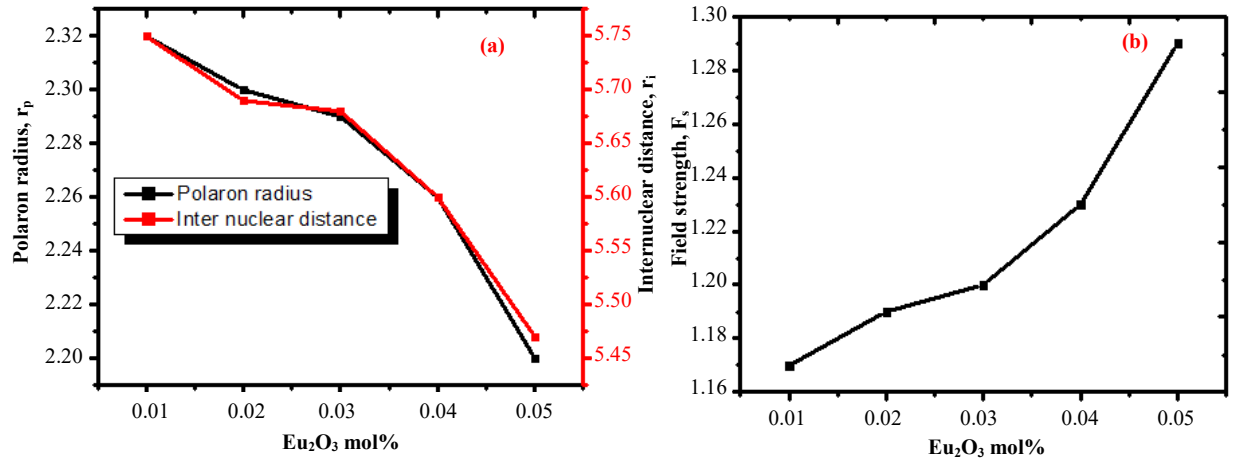

Figure 12 (a) Polaron radius and internuclear distance and (b) field strength of europium-doped soda-lime borosilicate glasses

3.4.4 Transmission Coefficient T and Reflection Loss R_L

Figure 13 illustrates the variation in the reflection loss and transmission coefficient of soda-lime borosilicate glass doped with europium oxide (Eu_2O_3). As the concentration of Eu^{3+} increases, the transmission coefficient rises and reflection loss decreases, indicating that the glasses become more optically transparent and less reflective. However, at higher dopant concentrations (0.04 – 0.05 Eu mol%), there is a decrease in the transmission coefficient and an increase in reflection loss, suggesting reduced optical transparency and increased reflectivity. These findings are in line with the reports of Umar et al. [20] and Aliyu et al. [28].

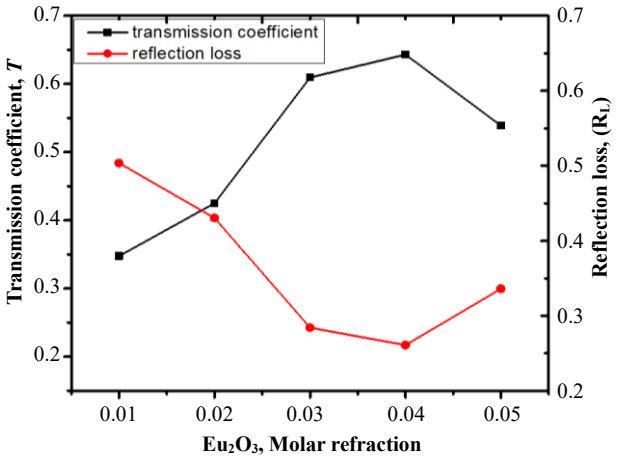

Figure 13 Transmission coefficient (*T*) and reflection loss (R_L) of europium-doped soda-lime borosilicate glasses

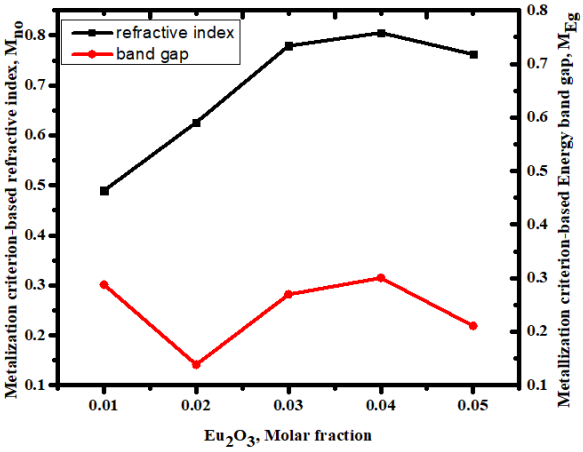

Figure 14 Variation of refractive index-based and optical band gap metallization criterion of Europium doped soda-lime borosilicate glasses

3.5 Metallization criterion based on band gap energy (M_{Eg}) and refractive index (M_{no})

The necessary conditions for a solid to be classified as metallic or non-metallic are determined by Herzfeld's 1927 theory of metallization [29], which states that Rm/Vm > 1 for metals and $R_m/V_m < 1$ for non-metals. The metallization criterion is defined as the difference from 1 or $M = 1 - \frac{R_m}{V_m}$ [30]. Furthermore, it was shown that typical insulators are materials with large, M close to 1. According to Umar et al. [20], the metallization criterion of any material reveals whether the material is insulating. Based on its band gap energy (E_g) and refractive index (n). Figure 14 displays the graphs for the Eu^{3+} doped borosilicate glass metallization criterion based on refractive index and optical band gap energy. Considering the band gap energy, the values are found in the range of 0.49-0.81, while the refractive index ranges from 0.09 to 0.31. In Figure 14, it was observed that the increasing concentration of Eu^{3+} reduces the metallization criterion of the glasses. This is due to the increasing number of refractive index (0.04-0.05Eu) and decreasing number of energy gaps (0.04-0.05Eu). The metallization criterion's decreasing value suggests that when Eu^{3+} increases, there is a tendency for metallization in the electronic structure of the glasses that are formed. The small value of the metallization criterion suggested that the width of both valence and conduction bands became widened which led to a narrow band gap and increased the possibility of glasses metalizing [30]. A similar decrease in the metallization criterion was observed and reported by Azlan et al. [68] and Meena [33] in their investigation.

3.6 Optical electronegativity χ

Optical electronegativity (χ) is a highly effective parameter for comprehending the chemical bonding structure of optical materials. Reddy et al. [32] claim that the size of χ reveals the kind of bonding between the materials. A substance is considered ionic if χ is

high, and covalent if χ is low. Additionally, it is observed that molecules with a lower χ value also have a higher refractive index [32]. Figure 15b shows that as the Eu^{3+} increases, the electronegativity of Eu_2O_3 doped glasses reduces. At some concentrations, the decrease in electronegativity suggests that the covalent nature of the glass material has increased [74].

3.7 Oxide ion polarizability and optical basicity of glass

The ability of oxide glass to contribute to the negative charges in the glass matrix is examined by the theoretical optical basicity (Λ). In other words, it describes the oxygen's capacity to donate electrons to the oxide glass [75]. Figure 15a shows the influence of Eu^{3+} concentration on the oxide ion electronic polarizability and optical basicity of the produced glass. The optical basicity and oxide ion polarizability for 0.04 - 0.05Eu mol/% doped glasses show an increasing trend with a significant increase in the optical basicity of the glasses. This could be attributed to the breaking of bonds leading to the structural change i.e., the decrease in bridging oxygens (BOs) by forming more non-bridging oxygen (NBOs) which makes the glasses more polarized. Increases in optical basicity indicate an increase in the ionic nature of the cation-oxygen bonds, which also means that the produced glass is basic. The high optical basicity demonstrates that oxide ions have a high electron-donating ability to the cations. These observations were also established in previous literature [16, 29, 75].

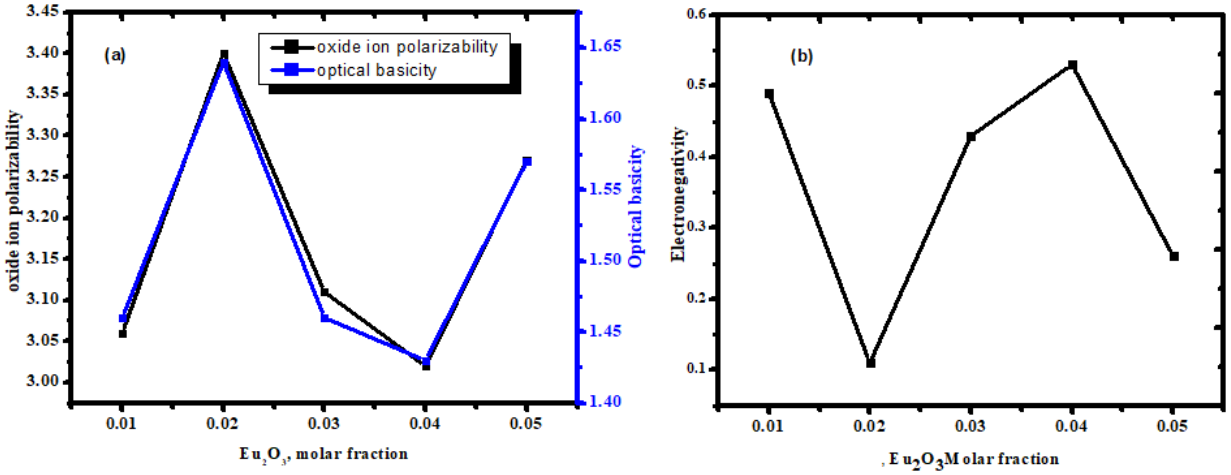

Figure 15 (a) Optical basicity (Λ) and oxide ion polarizability α_o^{2-} (b) optical electronegativity of europium doped soda-lime borosilicate glasses.

Table 3 presents a concise overview of the optimum glass produced in this study compared with other studies that used agricultural waste and conventional materials in glass production.

Table 3 A comparative analysis of the current study with the existing literature

Glass code	Properties	References
NaCaBSiEu	The wheat husk used in this study contains 88.65% silicate. The addition of europium ions increases glass density and molar volume. The higher Urbach energy suggests a glassy nature, while the metallization criterion shows that the samples do not exhibit metalizing properties.	Present study
Er-RHSBT	The study shows a notable yield of 98.55% silica from rice husk. Glass made from rice husk ash exhibits an increased optical band gap due to greater structural compactness. Additionally, higher concentrations of erbium ions decrease Urbach energy, indicating a strong link between ionic doping and the glass's optical properties.	[20]
BSBT	Rice husks have a silicate content of 98.62%. Additionally, glass density inversely correlates with molar volume as Er^{3+} ion concentration increases.	[22]
xEu2O3•(100 − x)[4PbO2•Pb]	The analysis of the glass samples showed significant variations in direct and indirect bandgap energies. A correlation was found between the refractive index and non-bridging oxygen, along with local density. Additionally, Urbach energy increased with higher concentrations of Eu^{3+} ions.	[71]

4. Conclusion

In conclusion, the study comprehensively investigated the europium-doped soda-lime borosilicate glass, revealing key insights into its physical, structural, and optical characteristics. Utilizing wheat husk ash (WHA) and calcined eggshell as glass precursors was validated through XRF analyses. FTIR spectroscopy identified important functional groups in the glass matrix, while XRD patterns confirmed its amorphous nature. The glass doped with a 0.05 mol% of Eu^{3+} exhibited the highest density, molar volume, and Urbach energy, alongside direct band gaps ranging from 3.55 to 4.90 eV. These properties indicate strong potential for UV-absorbing materials

or high-energy photonic devices. Conversely, the indirect optical band gap ranged from 0.40 to 1.99 eV, suggesting suitability for applications in lower-energy photonic devices like solar cells or infrared detectors. These findings underscore the versatility of europium-doped borosilicate glasses, particularly in advancing technologies such as white light-emitting diodes (LEDs) through their unique emission properties under various excitation wavelengths.

5. Acknowledgment

The authors express their profound gratitude to the Department of Mechanical and Civil Engineering at Nile University for their invaluable support during the experimental phase, which significantly contributed to the successful completion of this publication.

6. References

[1] Nandyala SH, Hungerford G, Santos JD, Walsh BM, Di Silvio L, Stamboulis A. Time-resolved and excitation-emission matrix luminescence behaviour of boro-silicate glasses doped with Eu^{3+} ions for red luminescent application. Mater Res Bull. 2021;140:111340.

[2] Tayal Y, Rao AS. Orange colour emitting Sm^{3+} ions doped borosilicate glasses for optoelectronic device applications. Opt Mater. 2020;107:110070.

[3] Li S, Liu H, Wu F, Chang Z, Yue Y. Effects of alkaline-earth metal oxides on structure and properties of iron phosphate glasses. J Non Cryst Solids. 2016;434:108-14.

[4] He X, Li C, Liu J, Huang Q, Shen X, Liu T, et al. Glass forming ability, structure and properties of Cr_2O_3-Fe_2O_3 codoped MgO-Al_2O_3-SiO_2-BO_3 glasses and glass ceramics. J Non Cryst Solids. 2020;529:119779.

[5] Anjaiah J, Laxmikanth C, Veeraiah N. Spectroscopic properties and luminescence behaviour of europium doped lithium borate glasses. Physica B Condens Matter. 2014;454:148-56.

[6] Goh KW, Wong YH, Ramesh S, Chandran H, Krishnasamy S, Ramesh S, et al. Effect of pH on the properties of eggshell-derived hydroxyapatite bioceramic synthesized by wet chemical method assisted by microwave irradiation. Ceram Int. 2021;47(7):8879-87.

[7] Mariselvam K, Kumar RA, Karthik S. Optical and luminescence characteristics of europium doped barium lithium fluoroborate glasses. Chem Phys. 2019;525:110379.

[8] Miniscalco WJ. Optical and electronic properties of rare earth ions in glasses. In: Digonnet MJF, editor. Rare-Earth-Doped Fiber Lasers and Amplifiers. 2nd ed. Taylor & Francis; 2001. p. 18-130.

[9] Luo P, Huang P, Wang J, Yao C, Zhao Y, Zhuo B, et al. Controllable synthesis of glass ceramic containing YF_3:Eu^{3+} nonocrystals: well-preserved Eu and prolong lifetime. J Am Ceram Soc. 2020;103(5):3089-96.

[10] Hegde V, Wagh A, Hegde H, Dwaraka Vishwanath CS, Kamath SD. Spectroscopic investigation on europium-doped heavy metal borate glasses for red luminescent application. Appl Phys A. 2017;123:302.

[11] Zhao J, Huang L, Xiao Z, Zhao S, Xu S. Luminescence properties of europium doped borosilicate glasses. Ceram Int. 2019;45(17):23804-7.

[12] Goodenough KM, Wall F, Merriman D. The rare earth elements: demand, global, resources and challenges for resourcing future generations. Nat Resour Res. 2018;27(2):210-6.

[13] Bulus I, Bhaktiar H, Hussin R, Danmallam IM, Ghoshal SK. Realization of efficient red laser using europium doped new boro-telluro-dolomite glass hosts: Ag nanoparticles functionality. J Phys: Conf Ser. 2020;1484:012019.

[14] Dwaraka Viswanath CS, Venkata Krishnaiah K, Jayasankar CK. Luminescence properties of europium-doped oxyfluorosilicate glasses for visible light devices. Opt Mater. 2018;83(3):348-55.

[15] Kaur S, Vishwakarma AK, Deopa N, Prasad A, Jayasimhadri M, Rao AS. Spectroscopic studies of Dy^{3+} doped borate glasses for cool white light generation. Mater Res Bull. 2018;104:77-82.

[16] Elkholy H, Othman H, Hager I, Ibrahim M, de Ligny D. Europium-doped tellurite glasses: the Eu^{2+} emission in tellurite, adjusting Eu^{2+} and Eu^{3+} emissions toward white light emission. Materials (Basel). 2019;12(24):4140.

[17] Komatsu T, Dimitrov V, Tasheva T, Honma T. Electronic polarizability in silicate glasses by comparison of experimental and theoretical optical basicities. Int J Appl Glass Sci. 2021;12(3):424-42.

[18] Gowda GVJ, Devaraja C, Eraiah B, Dahshan A, Nazrin SN. Structural, thermal and spectroscopic studies of Europium trioxide doped lead boro-tellurite glasses. J Alloys Compd. 2021;871:159585.

[19] Mariselvam K, Arun Kumar R, Karthik S. Optical and luminescence characteristics of europium doped barium lithium fluoroborate glasses. Chem Phys. 2019;525:110379.

[20] Umar SA, Halimah MK, Chan KT, Latif AA. Physical, structural and optical properties of erbium doped rice husk silicate borotellurite (Er-doped RHSBT) glasses. J Non Cryst Solids. 2017;472:31-8.

[21] Pa FC, Chik A, Fazlul Bari M. Palm ash as an alternative source for silica production. MATEC Web Conf. 2016;78:01062.

[22] Hamza AM, Halimah MK, Muhammad FD, Chan KT. Physical properties, ligand field and Judd-Ofelt intensity parameters of bio-silicate borotellurite glass system doped with erbium oxide. J Lumin. 2019;207:497-506.

[23] Agbabiaka OG, Oladele IO, Akinwekomi AD, Adediran AA, Balogun AO, Olasunkanm OG, et al. Effect of calcination temperature on hydroxyapatite developed from waste poultry eggshell. Sci Afr. 2020;8:e00452.

[24] Razali N, Musa FA, Jumadi N, Jalani AY. Production of calcium oxide from eggshell: study on calcination temperature, raw weight and contact time. RSU International Research Conference 2021; 2021 Apr 30; Pathum Thani, Thailand. Thailand: RSU; 2021. p. 624-37.

[25] Mariselvam K, Arun Kumar R, Rajeswara Rao V. Concentration-dependence and luminescence studies of erbium-doped barium lithium fluoroborate glasses. Opt Laser Technol. 2019;118:37-43.

[26] Khan I, Rooh G, Rajaramakrishna R, Srisittipokakun N, Kim HJ, Kirdsiri K, et al. Luminescence characteristics of Sm^{3+}-doped lithium barium gadolinium silicate glasses for Orange LED's. Spectrochim Acta A: Mol Biomol Spectrosc. 2019;214:14-20.

[27] Rittisut W, Wantana N, Ruangtaweep Y, Mool-am-kha P, Rujirawat S, Manyum P, et al. The radioluminescence and photoluminescence behavior of lithium alumino borate glasses doped with Tb_2O_3 and Gd_2O_3 for green luminescence applications. Opt Mater. 2021;121:111437.

[28] Aliyu US, Kamari HM, Geidam IG, Alade IO, Noorazlan AM, Hamza AM, et al. Spectroscopic investigations of Er_2O_3 doped silica borotellurite glasses. Opt Mater. 2021;114:110987.
[29] Halimah MK, Faznny MF, Azlan MN, Sidek HAA. Optical basicity and electronic polarizability of zinc borotellurite glass doped La^{3+} ions. Results Phys. 2017;7:581-9.
[30] Dimitrov V, Komatsu T. An interpretation of optical properties of oxides and oxide glasses in terms of the electronic ion polarizability and average single bond strength. J Univ Chem Technol Metallurgy. 2010;45(3):219-50.
[31] Singh D, Singh S, Singh T, Kaur P. Samarium and gadolinium-co-doped lead borate glasses for luminescent applications. J Mater Sci: Mater Electron. 2021;32(6):6900-11.
[32] Reddy RR, Nazeer Ahammed Y, Rama Gopal K, Raghuram DV. Optical electronegativity and refractive index of materials. Opt Mater. 1998;10(2):95-100.
[33] Meena SL. Thermal and physical properties of Pm^{3+} ions doped lead lithium bismuth silicate glasses. J Pure Appl Ind Phys. 2019;9(11):72-81.
[34] Dimitrov V, Sakka S. Linear and nonlinear optical properties of simple oxides II. J Appl Phys. 1996;79(3):1741-5.
[35] Moustafa ES, Elkhateb F. The estimation of the oxide ion polarizability using electronegativity for B_2O_3-Li_2O-Mo glass system. Chem Mater Sci. 2012;2(1):25-31.
[36] Zhao X, Wang X, Lin H, Wang Z. Correlation among electronic polarizability, optical basicity and interaction parameter of Bi_2O_3-B_2O_3 glasses. Physica B Condens Matter. 2007;390(1-2):293-300.
[37] Reddy RR, Nazeer Ahammed Y, Abdul Azeem P, Rama Gopal K, Rao TVR. Electronic polarizability and optical basicity properties of oxide glasses through average electronegativity. J Non Cryst Solids. 2001;286(3):169-80.
[38] Moustafa ES, Elkhateb F. The estimation of the oxide ion polarizability for B_2O_3-Li_2O-Mo glass system. Am J Appl Sci. 2012;9(3):446-9.
[39] Shaaban KS, Abdel Wahab EA, El-Maaref AA, Abdelawwad M, Shaaban ER, Yousef ES, et al. Judd – Ofelt analysis and physical properties of erbium modified cadmium lithium gadolinium silicate glasses. J Mater Sci: Mater Electron. 2020;31:4986-96.
[40] Tangboriboon N, Kunanuruksapong R, Sirivat A. Preparation and properties of calcium oxide from eggshells via calcination. Mater Sci-Pol. 2012;30(4):313-22.
[41] Awogbemi O, Inambao F, Onuh EI. Modification and characterization of chicken eggshell for possible catalytic applications. Heliyon. 2020;6(10):e05283.
[42] Witoon T. Characterization of calcium oxide derived from waste eggshell and its application as CO_2 sorbent. Ceram Int. 2011;37(8):3291-8.
[43] Ahmad W, Sethupathi S, Munusamy Y, Kanthasamy R. Valorization and calcined chicken eggshell for sulphur dioxide and hydrogen sulfide removal at low temperature. Catalysts. 2021;11(2):295.
[44] Habte L, Shiferaw N, Mulathi D, Thenepalli T, Chilakala R, Ahn JW. Synthesis of nanocalcium oxide from waste eggshell by sol-gel method. Sustainability. 2019;11(11):3196.
[45] Terzioğlu P, Yücel S, Kuş Ç. Review on a novel biosilica source for production of advanced silica-based materials: wheat husk. Asia-Pac J Chem Eng. 2019;14(1):e2262.
[46] Gouran A, Aghel B, Nasirmanesh F. Biodiesel production from waste cooking oil using wheat bran ash as a sustainable biomass. Fuel. 2021;295:120542.
[47] Ershard M, Ali A, Mehta NS, Singh RK, Singh SK, Pyare R. Mechnaical and biological response of (CeO_2+La_2O_3)-substituted 45S5 bioactive glasses for biomedical application. J Aust Ceram Soc. 2020;56(4):1243-52.
[48] Zaid MHM, Sidek HAA, El-Mallawany R, Almasri KA, Matori KA. Synthesis and characterization of samarium doped calcium soda-lime-silicate glass derived wollastonite glass-ceramics. J Mater Res Technol. 2020;9(6):13153-60.
[49] Saddeek YB, Shaaban ER, Moustafa ES, Moustafa HM. Spectroscopic properties, electronic polarizability, and optical basicity of Bi_2O_3-Li_2O-B_2O_3 glasses. Physica B Condens Matter. 2008;403(13-16):2399-407.
[50] Muniz RF, Soares VO, Montagnini GH, Medina AN, Baesso ML. Thermal, optical and structural properties of relatively depolymerized sodium calcium silicate glass and glass-ceramic containing CaF_2. Ceram Int. 2021;47(17):24966-72.
[51] Chanthima N, Kaewkhao J. Properties of erbium luminescence in barium borophosphate glasses. Mater Today: Proc. 2017;4(5):6099-104.
[52] Acikgoz A, Ceyhan G, Aktas B, Yalcin S, Demircan G. Luminescent, structural and mechanical properties of erbium oxide doped natural obsidian glasses. J Non Cryst Solids. 2021;572:121104.
[53] Kaur R, Khanna A, González-Barriuso M, González F, Chen B. Structural, optical and thermal properties of glass and anti-glass phases in strontium tellurite and borotellurite systems doped with europium. Mater Res Bull. 2018;106:288-95.
[54] Abdel Wahab EA, Shaaban KS, Yousef ES. Enhancement of optical and mechanical properties of sodium silicate glasses using zirconia. Opt Quant Electron. 2020;52(10):458.
[55] Deepa M, Doddoji R, Dwaraka Viswanath CS, Chandrasekhar AV. Optical and NIR luminescence spectral studies: Nd^{3+}-doped borosilicate glasses. J Lumin. 2019;213:191-6.
[56] Abou Hussein EM, Shaban SE, Rammah YS, Hamed Misbah M, Marzouk MA. Newly developed CeO_2 and Gd_2O_3-reinforced borosilicate glasses from municipal waste ash and their optical, structural, and gamma-ray shielding properties. Sci Rep. 2024;14:13673.
[57] Gao G, Wei J, Shen Y, Peng M, Wondraczek L. Heavily Eu_2O_3-doped yttria-aluminoborate glasses for red photoconversion with a high quantum yield: luminescence quenching and statistics of cluster formation. J Mater Chem C. 2014;2(41):8678-82.
[58] Saraf R, Shivakumara C, Behera S, Nagabhushana H, Dhananjaya N. Photoluminescence, photocatalysis and Judd–Ofelt analysis of Eu^{3+}-activated layered BiOCl phosphors. RSC Adv. 2015;5:4109-20.
[59] Ebendorff-Heidepriem H, Ehrt D. Formation and UV absorption of cerium, europium and terbium ions in different valencies in glasses. Opt Mater. 2000;15(1):7-25.
[60] Shaaban SM, Al-Ghamdi H, Alsaif NAM, Rammah YS, Khattari ZY, Shams MS, et al. The role of Eu^{3+} ions on FTIR, UV–vis spectroscopy, photoluminescence, and mechanical properties of newly fabricated borate-based glasses. J Aust Ceram Soc. 2024;60(2):543-51.
[61] Ari J, Cavillon M, Plantevin O, Lancry M, Poumellec B. Europium spectroscopic properties impacted by femtosecond laser 3D nanostructuring in lithium niobium borosilicate glasses. Opt Mater: X. 2022;16:100198.

[62] Zikriya M, Renuka CG, Manjunath C. Optical absorption intensity analysis using Judd-Ofelt theory and photoluminescence investigation for red-emitting Eu^{3+}: TiO_2 nanoparticles. Solid State Sci. 2020;107:106371.
[63] Kremenovic A, Bozanic DK, Welsch AM, Jancar B, Nikolic AS, Boskovic M, et al. Effects of Eu^{3+} concentration on structural, optical and vibrational properties of multifunctional Ce(1−x)Eu(x)O2−delta) nanoparticles synthesized by thermolysis of 2,4-pentanedione complexes. J Nanosci Nanotechnol. 2012;12(12):8893-9.
[64] Barde RV. Influence of CeO_2 content on complex optical parameters of phosphovanadate glass system. Spectrochim Acta A: Mol Biomol Spectrosc. 2016;153:160-4.
[65] Saadati M, Akhavan O, Fazli H. Single-layer MoS_2-MoO_3-x heterojunction nanosheets with simultaneous photoluminescence and co-photocatalytic features. Catalysts. 2021;11(12):1445.
[66] Schwarting M, Siol S, Talley K, Zakutayev A, Phillips C. Automated algorithms for band gap analysis from optical absorption spectra. Mater Discov. 2017;10:43-52.
[67] Bajaj R, Rao AS, Vijaya Prakash G. Photoluminescence down-shifting studies of thermally stable Eu^{3+} ions doped borosilicate glasses for visible red photonic device applications. J Non Cryst Solids. 2022;575:121184.
[68] Azlan MN, Halimah MK, Shafinas SZ, Daud WM. Polarizability and optical basicity of Er^{3+} ions doped tellurite based glasses. Chalcogenide Letters. 2014;11(7):319-35.
[69] Kesavulu CR, Kim HJ, Lee SW, Kaewkhao J, Wantana N, Kothan S, et al. Influence of Er^{3+} ion concentration on optical and photoluminescence properties of Er^{3+}-doped gadolinium-calcium silica borate glasses. J Alloys Compd. 2016;683:590-8.
[70] Nabilah Razali NA, Mustafa IS, Azman NZN, Kamari HM, Rahman AA, Rosli K, et al. The physical and optical studies of erbium doped borosilicate glass. J Phys: Conf Ser. 2018;1083:012004.
[71] Zagrai M, Suciu RC, Rada S, Pică ME, Pruneanu S. Structural and optical properties of Eu^{3+} ions in lead glass for photonic applications. J Non Cryst Solids. 2021;569:120988.
[72] Hassib MD, Kaky KM, Kumar A, Şakar E, Sayyed MI, Baki SO, et al. Boro-silicate glasses co-doped Er^{+3}/Yb^{+3} for optical amplifier and gamma radiation shielding applications. Physica B Condens Matter. 2019;567:37-44.
[73] Mhareb MHA, Hashim S, Ghoshal SK, Alajerami YSM, Saleh MA, Maqableh MMA, et al. Optical and erbium ion concentration correlation in lithium magnesium borate glass. Optik. 2015;126(23):3638-43.
[74] Hassan MA. Effect of halides addition on the ligand field of chromium in alkali borate glasses. J Alloys Compd. 2013;574:391-7.
[75] Kashif I, Ratep A, Adel G. Polarizability, optical basicity and optical properties of $SiO_2B_2O_3Bi_2O_3TeO_2$ glass system. Appl Phys A. 2018;124:486.